Lobanov, S., Daly, J. A., Goncharov, A. F., Chan, X., Ghose, S. K., Zhong, H., Ehm, L., Kim, T., Parise, J. B. (2018 online): Iodine in Metal–Organic Frameworks at High Pressure. - *Journal of Physical Chemistry A*.

DOI: http://doi.org/10.1021/acs.jpca.8b05443

# Iodine in Metal Organic Frameworks at High Pressure

Sergey S. Lobanov[†,‡,*], John A. Daly[§], Alexander F. Goncharov[‖], Xiaojun Chan[⊥], Sanjit K. Ghose[#], Hui Zhong[○], Lars Ehm[†,#], Taejin Kim[⊥], John B. Parise[†,§,○]

[†]Department of Geosciences, Stony Brook University, Stony Brook, NY 11794, USA

[‡]GFZ German Research Center for Geosciences, Section 4.3, Telegrafenberg, 14473 Potsdam, Germany

[§]Department of Chemistry, Stony Brook University, Stony Brook, NY 11794, USA

[‖]Geophysical Laboratory, Carnegie Institution of Washington, Washington, DC 20015, USA

[⊥]Department of Materials Science and Chemical Engineering, Stony Brook University, Stony Brook, NY 11794, USA

[#]Synchrotron Light Source II, Brookhaven National Laboratory, PO Box 5000, Upton, NY 11973, USA

[○]Joint Photon Sciences Institute, Stony Brook University, Stony Brook, NY 11794, USA

**Abstract**

Capture of highly-volatile radioactive iodine is a promising application of metal organic frameworks (MOFs), thanks to their high porosity with flexible chemical architecture. Specifically, strong charge-transfer binding of iodine to the framework enables efficient and selective iodine uptake as well as its long-term storage. As such, precise knowledge of the electronic structure of iodine is essential for a detailed modelling of the iodine sorption process, which will allow for rational design of iodophilic MOFs in the future. Here we probe the electronic structure of iodine in MOFs at variable iodine···framework interaction by Raman and optical absorption spectroscopy at high pressure (*P*). The electronic structure of iodine in the straight channels of SBMOF-1 (*Ca-sdb, sdb = 4,4`-sulfonyldibenzoate*) is modified irreversibly at $P > 3.4$ GPa by charge-transfer, marking a polymerization of iodine molecules into a 1D polyiodide chain. In contrast, iodine in the sinusoidal channels of SBMOF-3 (*Cd-sdb*) retains its molecular ($I_2$) character up to at least 8.4 GPa. Such divergent high-pressure behavior of iodine in the MOFs with similar port size and chemistry illustrates adaptations of the electronic structure of iodine to channel topology and strength of the iodine···framework interaction, which can be used to tailor iodine-immobilizing MOFs.

## 1. INTRODUCTION

Metal organic frameworks (MOFs) are synthetic porous solids with crystal structures made of two principal units: an organic linker and metal cluster. In constructing MOFs one has virtually endless flexibility to select linkers and metals to tailor frameworks for a specific application. As a result, thousands of MOFs are known to date with diverse physical and chemical properties that promise novel solutions for many grand challenges of the modern world, including selective gas sorption and storage.[1] Of special interest is the use of MOFs for air purification owing to their high porosity and tunable chemical architectures which allow MOFs to outperform classical sorbents, such as zeolites and activated carbons, in the ability to trap toxic chemicals.[2] One example is the use of MOFs for capturing radioactive iodine formed upon fission of nuclear fuel, which has been notably challenging to immobilize due to its volatility.[3] Iodophilic MOFs may enable next generation techniques for reprocessing of used nuclear fuel, but fundamental aspects that govern iodine adsorption are poorly understood. Here we explored the effect of channel topology on the MOF-iodine interaction with the aim to improve iodine capture by MOFs.

The iodine sorption capacity of many MOFs has been evaluated by exposing activated frameworks to iodine gas while monitoring the change in their weight.[4-10] Several high surface area (>1500 $m^2/g$) and large pore size (>10 Å) MOFs showed remarkable iodine uptake of more than 100 wt % and a packing density of ~2 $g/cm^3$, surpassing the industrially used materials, such as silver-bearing complexes[3], by a factor of 5-10.[4-5, 8] Surface area and pore size, however, appear to be of secondary importance as the MFM-300 MOF series showed an even higher packing density (~3 $g/cm^3$) within smaller (~8 Å) pores and the surface areas of ~1000-1200 $m^2/g$.[9] Moreover, alternative porous compounds with much smaller surface areas (~10 $m^2/g$) have comparable capacities[11-12]. Even nonporous compounds can host up to 20 wt % of $I_2$.[13]

Falaise, et al. provided the first systematic insights into the primary factors governing iodine uptake by focusing on the MIL-53 MOF series with variable pore functionalization.[6] MIL-53-x decorated with electron-donating groups, such as $NH_2$, showed the highest iodine uptake while its non-functionalized form performed the worst despite having a higher surface area (~1100 $m^2/g$). Subsequent studies confirmed the importance of charge-transfer (CT) interactions for iodine adsorption by porous solids.[9, 12, 14-15] In similarity to MOFs, increased iodine solubility has been observed in strong organic donors that form molecular CT complexes with iodine.[16-17] In fact, one can think of iodine adsorbed in a MOF as of an iodine-bearing molecular CT complex.

The electronic structure of iodine in molecular complexes is perturbed by CT resulting in characteristic spectroscopic features that are not observed in pure iodine or its solvents.[18] These

spectroscopic signatures provide reliable means to detect and characterize the strength of CT in iodine-bearing systems.[16, 19-20] Quantum-mechanical treatment of bonding in molecular CT complexes successfully reproduced these signatures and predicted that the donor-acceptor spatial separation, which can be controlled by pressure, governs the strength of their interaction.[21] This prediction found experimental confirmation in the limit of 0.5 GPa.[16, 22]

It is worth noting that the electronic structure of iodine itself is very sensitive to external pressure. For example, molecular iodine dissociates to an atomic metal through an intermediate incommensurate phase where I-I bonds continuously vary in the 2.86-3.11 Å range.[23] Bond distances in the incommensurate phase are typical of polyiodides[24], which themselves are energetically favored at high pressure due to its tendency to increase coordination.[25] Molecular-orbital representation of bonding in polyiodides suggests that they are stabilized by CT interaction of neighboring iodine species ($I_2$, $I^-$, $I_3^-$).[24] If polyiodides are present in MOFs, the CT interaction intrinsic to their bonding must compete with the iodine⋯framework binding CT interaction, and can affect iodine adsorption in the MOFs. Studies at high pressure provide a unique insight into this competition, as it allows isochemical tuning of the $I_2$⋯framework and $I_2$⋯$I_2$ interactions within iodine-filled MOFs, with implications for improving iodine uptake and selectivity. In addition, precise knowledge of the electronic structure of iodine species in MOFs is required for any thermodynamic modelling of their uptake kinetics and sorption selectivity. However, modelling work intended to locate iodine in powder diffraction studies, often hypothesizes the presence of molecular $I_2$ only[4-5], although the presence of polyiodide species in MOFs has been established by single crystal structural determination.[26-27] Optical and Raman spectroscopy provide unique insights into the electronic structure, chemical reactions, and changes in iodine speciation in the pores. However, these techniques have been largely underused in characterizing iodine in MOFs.

Here we used Raman and optical electronic spectroscopy in combination with powder x-ray diffraction (PXRD) to probe the electronic structure of iodine in MOFs as a function of pressure. We compressed two structurally different MOFs (SBMOF-1 and SBMOF-3, SB for Stony Brook University) that are based on *sdb* (*4,4`-sulfonyldibenzoate*) linker and an octahedrally-coordinated metal. Both SBMOF-1 (*Ca-sdb*) and SBMOF-3 (*Cd-sdb*) are monoclinic ($P2_1/n$ and $C_2/c$), have similar pore size (~7 Å) and its chemical decoration, but differ in having straight and sinusoidal channels, respectively (Fig. 1).[28-29] This diversity allows isolation of the effect of pore geometry on the donor-acceptor exchange between iodine species and the wall sites of the pore. Surprisingly, we found that iodine in SBMOF-1 is perturbed by CT at high pressure, while iodine in SBMOF-3 remains intact. In the case of I@SBMOF-1, the mechanism of the pressure-induced CT is complex with donor contributions not only from the

linker but also from neighboring iodine molecules that get activated at high pressure, leading to their aggregation into polyiodides.

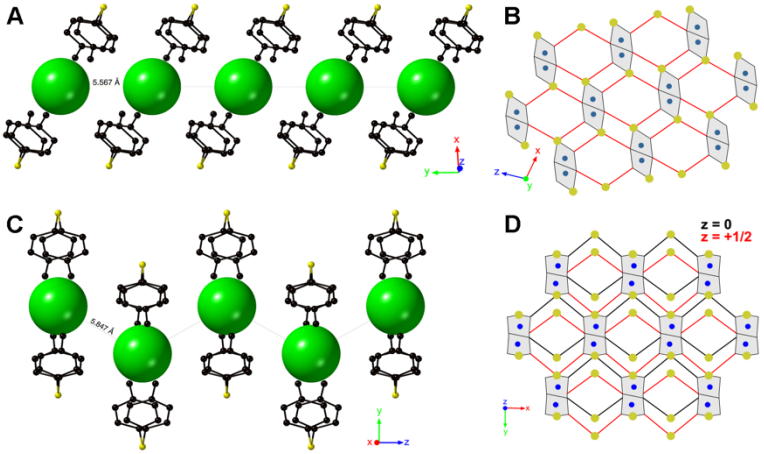


**Figure 1**. Straight channels in SBMOF-1(**A**) and sinusoidal in SBMOF-3 (**C**). Carbon atoms are black and sulfur is yellow. Oxygen, hydrogen, and calcium/cadmium atoms are omitted for clarity. Large green spheres depict iodine sorption sites. (**B**): 'Wine-rack' topology of SBMOF-1. Red line is the *sdb* linker with all sulphonyl groups (yellow) bonded with Ca to form $CaO_6$-octahedra (grey). All carboxyls also participate in $CaO_6$-ocathedra and are not shown for clarity. (**D**): 'Wine-rack' topology of SBMOF-3. Black (z = 0) and red (z = 1/2) lines are the *sdb* linker with only half sulphonyl groups bonded with Cd to form $CdO_6$-octahedra (grey). All carboxyls also participate in $CdO_6$ and are not shown for clarity.

## 2. EXPERIMENTAL METHODS

### 2.1 Synthesis and iodine loading

Single crystals of SBMOF-1 and SBMOF-3 were synthesized under solvothermal conditions following the previously reported protocols.[10, 28-29] Subsequently, MOFs were activated by heating in air at ~250 °C for ~12 h, and then exposed to dry iodine gas for 2 days in a sealed chamber containing iodine crystals, similarly to our report on the iodine uptake by SBMOFs.[10]

### 2.2 Diamond anvil cell loadings

Almax plate DAC with diamond culets of 400 μm were used to generate high pressure. Stainless steel foil with the initial thickness of 100 μm was indented to 40-60 μm by pressing on the foil with the diamond anvils. A 250 μm hole was drilled in the center of the indentation to serve as a sample chamber. Subsequently, the gasket was sonicated in ethanol for 30 min, dried, and then positioned between the anvils. For all spectroscopic measurements high-quality single crystals of I@SBMOF-1 and I@SBMOF-3 (and their activated forms) were positioned inside the sample chamber filled with silicon oil, serving as a non-penetrating pressure-transmitting medium. In PXRD experiments, powders of the MOFs were loaded and the remaining sample chamber volume was filled with silicon oil. All experiments were conducted at 300 K. Ruby was used as a pressure gauge.[30]

### 2.3 Raman spectroscopy

Unpolarized Raman spectra were excited with a single mode wavelength stabilized 785 nm laser (I0785S50100B, Innovative Photonic Solutions, NJ) operating at ~2.5 mW. No laser-induced changes were evident at such relatively low laser power as confirmed by a test run at 0.05 mW laser power. The choice of the 785-nm excitation was important as I@SBMOF-1 and I@SBMOF-3 have negligible absorbencies at this wavelength at 1 atm, suppressing sample heating and possible light-induced changes. The laser was focused by a Leica DM2500M microscope as part of the Renishaw inVia Raman system. Backscattered radiation was collected by the same optical path, focused onto a 1200 line/mm diffraction grating, and passed to an air-cooled CCD. Raman spectra were typically collected in the 50-2000 $cm^{-1}$ range with an overall exposure of 5-10 minutes. The spectra resolution was about 1 $cm^{-1}$. In addition, a 514-nm excitation of a He-Ne laser was used to excite ruby fluorescence, which was necessary for pressure measurements in the DAC (ruby fluorescence is at ~695 nm; thus cannot be excited by a 785-nm laser). All spectra were measured at room temperature.

### 2.4 Electronic spectroscopy

Absorption spectra were collected by a custom-built microscope designed for optical measurements in a DAC.[31] Chromatic aberrations were minimized by all-reflective optics and the relatively small aberrations introduced by diamond anvils[32], were accounted for by collecting a reference spectrum through the pressure medium. A fiber-coupled halogen-deuterium lamp (350-1100 nm) focused to a ~50 μm spot on the sample served as a probe. The central portion of the transmitted radiation (~20 μm) was projected onto the entrance slit of the Acton Research Corporation Spectra Pro 500-i spectrometer (300 grooves/mm) sensitive in the near-ultraviolet (UV), visible, and near-infrared (IR) range. All spectra were collected for 0.25 s at five different grating positions and then stitched together to produces a final spectrum. Samples absorbance was evaluates as: $A(\nu) = -log_{10}(I_{sample} - I_{bckg})/(I_{reference} - I_{bckg}))$, where $I_{sample}$ is the intensity of light transmitted through the sample, $I_{reference}$ is the intensity of light passed through the pressure medium, and $I_{bckg}$ is the background reading. All spectra were collected at room temperature.

### 2.5 Synchrotron powder x-ray diffraction (PXRD)

PXRD experiments were conducted at Beamline 28-ID-2 of NSLS-II. X-ray beam (52.38 keV) was collimated to ~0.3 x 0.2 $mm^2$ to minimize the contribution of gasket to the diffraction pattern. The diffraction patterns were collected on a Perkin-Elmer amorphous silicon flat-panel detector (2048x2048 pixels with a 200 x 200 $\mu m^2$ pixel size). The contributions from the diamond anvils to the scattering signal were carefully masked prior to the conversion from two-dimensional to one-dimensional diffraction patterns. For the determination of the geometric

parameters from a $CeO_2$ (NIST 674b) standard and the radial integration of the two-dimensional data the program FIT2D was used.[33]

## 3. RESULTS

The absorption spectrum of $I_2$ in inert organic solvents is dominated by bands at ~540 nm ($^1\Sigma_{0+g} \rightarrow {}^3\Pi_{0+u}$, B state) and ~515 nm ($^1\Sigma_{0+g} \rightarrow {}^1\Pi_u$, C state)[34-37], which account for about 95 % of light extinction in the visible range.[37] Additionally, a band at ~680 nm ($^1\Sigma_{0+g} \rightarrow {}^3\Pi_{1u}$, A state) is dipole-allowed and may appear as a shoulder on the main absorption peak accounting for ~5 % of its intensity. In weakly interacting solvents, such as benzene, the B and C bands are blue-shifted to ~500 nm and their individual components are hard to resolve because of the overlap.[16] The single iodine sorption site in I@SBMOF-1 is in the vicinity of the phenyl ring with $I_2$ oriented nearly perpendicular to the plane of the organic group[10]. Such a conformation resembles that found in other iodine-benzene systems[38]; thus, I@SBMOF-1 is expected to bear spectroscopic similarities with iodine in benzene, a well-studied system at near ambient conditions. With the same linker, I@SBMOF-3 might show a similar spectroscopic behavior.

Figure 2A shows pressure-induced changes in the optical absorption of I@SBMOF-1. At 0.3 GPa, the only major absorption feature is the asymmetric band centered at ~500 nm. Its assignment to the B and C states of $I_2$ is straightforward. A-band is not resolved, due to the thin sample of ~10-20 μm, as required by small sample volumes required for diamond anvil cell (DAC) loadings. Please note, that we did not identify individual components of the overlapping B and C bands, which is adequate because these states are triplet and singlet states of the $\pi_g^* \rightarrow \sigma_u^*$ transition and the spectral position of this band is a convenient and sufficient way to characterize pressure-induced changes to the $\pi_g^* - \sigma_u^*$ energy gap.[34] In addition, it has been shown that the deconvolution of iodine absorption spectrum into the components is highly sensitive to the fitting model.[36-37] Below 400 nm and extending into the UV range is the absorption edge that is only present in iodine-loaded SBMOF-1. Iodine-free SBMOF-1 and $I_2$ are fairly transparent at 330-400 nm (Suppl. Fig. S1)[35-37]; hence, the assignment of the absorption edge in I@SBMOF-1 to the *sdb*-$I_2$ CT band.[16, 39] The presence of CT band in the spectra of I@SBMOF-1 is a direct spectroscopic evidence of a donor-acceptor binding of iodine to the framework of SBMOF-1. Upon compression to 2.2 GPa, the position and width of the 500-nm band remain unchanged, as does the contribution of the *sdb*-$I_2$ CT band, manifesting together a constant iodine···framework CT interaction in this pressure range. At 3.4 GPa, the 500-nm band is slightly broadened and is less intense. At the same time, the CT band is intensified (red-shifted) abruptly and starts overlapping with the 500-nm band. Surprisingly, a very similar spectroscopic discontinuity is observed in iodine-free SBMOF-1 (Suppl. Fig. S1), indicating that

the increased absorbance at < 400 nm in the iodine-loaded sample cannot be attributed solely to the intensification of the CT band and is at least partially related to a pressure-induced transformation in the MOF framework. At 4.8 GPa, the main absorption band is split into several components below and above the center at 500 nm. The splitting increases upon further compression and two components are clearly resolved at 7.5 GPa with centers at 455 and 600 nm, while the 500-nm peak is no longer present. In contrast to SBMOF-1, absorption spectra of SBMOF-3 do not change with pressure: the frequency and intensity of the 500-nm band as well as that of the CT absorption edge remain largely unchanged over the entire compression cycle to 7.5 GPa (Fig. 2B).

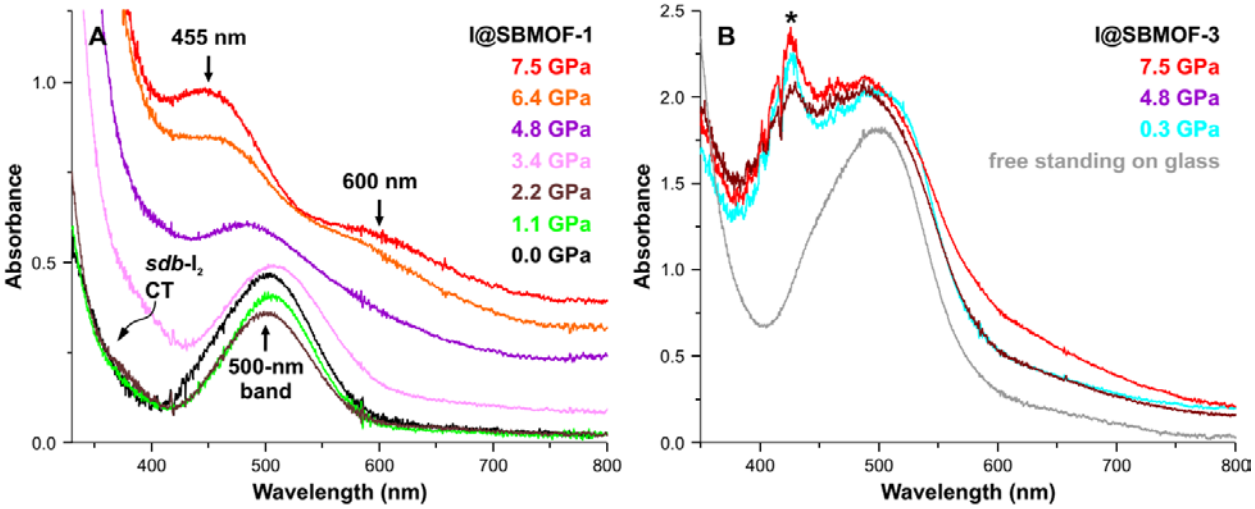


**Figure 2**. Absorption spectra of I@SBMOF-1 (**A**) and I@SBMOF-3 (**B**) measured upon compression to 7.5 GPa. Asterisk in (**B**) marks a spurious peak due to low intensity of the light source and poor sensitivity of the detector below 500 nm. For comparison, we show a spectrum of I@SBMOF-3 collected at a longer accumulation and outside diamond anvil cell (grey) that does not show the spurious peak.

Raman spectroscopy further confirms the different high-pressure behavior of iodine in the SBMOFs. At 1.1 GPa, molecular iodine in I@SBMOF-1 gives rise to a narrow peak at 210 $cm^{-1}$ (labeled m-$I_2$) (Fig. 3), characteristic of molecular (m) iodine in weak organic solvents.[40] No overtones are observed for this band as the Raman excitation wavelength (785 nm) provides a non-resonance scattering regime. The frequency of m-$I_2$ band increases continuously to 3.6 GPa ($dv/dP$ = 4.8 $cm^{-1}$/GPa). The observed frequency shift is ~2.5 times higher than that observed in solid iodine (1.8 $cm^{-1}$/GPa at $P$ > 3 GPa);[41] revealing an anomalously strong stiffening of the I-I bond in the straight channels of I@SBMOF-1 with pressure. Such a strong frequency shift suggests a rapid decrease of the I-I bond length and indicates that the bond is not perturbed by CT to the strongly antibonding $\sigma_u^*$ orbital of $I_2$ as it would inevitably loosen the bond strength. At $P$ > 3.6 GPa, the m-$I_2$ band cannot be clearly resolved. Instead, a new intense and broad peak centered at ~160 $cm^{-1}$ and a shoulder at ~190 $cm^{-1}$ appear in the Raman spectra.

The new bands are about an order of magnitude more intense than the m-$I_2$ band and further intensify with compression. The width and position of the 160-190 $cm^{-1}$ feature are both similar to that observed in iodine molecular complexes with strong organic donors,[20] where the decreased frequency of I-I stretching is attributed to the CT interaction of the donor with the $\sigma_u^*$ orbital of $I_2$.[42] Interestingly, polyiodides containing $I_2$ perturbed by CT with an $I_n^-$ ($n$ = 1, 3, 5, *etc.*) donor show indistinguishable Raman bands.[42-43] Following these previous studies, we assigned the broad 160-190 $cm^{-1}$ band to molecular iodine perturbed by CT interactions and labeled it as p-$I_2$. At 8.4 GPa, yet another new peak appeared at ~110 $cm^{-1}$ and can be assigned to $I_3^-$ or $I_2^-$.[24, 42-44] At the highest pressure (8.4 GPa), the p-$I_2$ band is ~100 times more intense than the m-$I_2$ band at 1 atm. In addition, a progression of overtones is observed for p-$I_2$, suggesting a resonance-like enhancement of the higher order transitions, just as expected from the I@SBMOF-1 absorption spectra measured at P > 4 GPa (Fig. 2A) which show strong absorption at the Raman excitation wavelength of 785 nm. The p-$I_2$ band is preserved on decompression to 1 atm, implying an irreversible character of the pressure-induced transformations in the electronic structure of iodine (Suppl. Fig. S2).

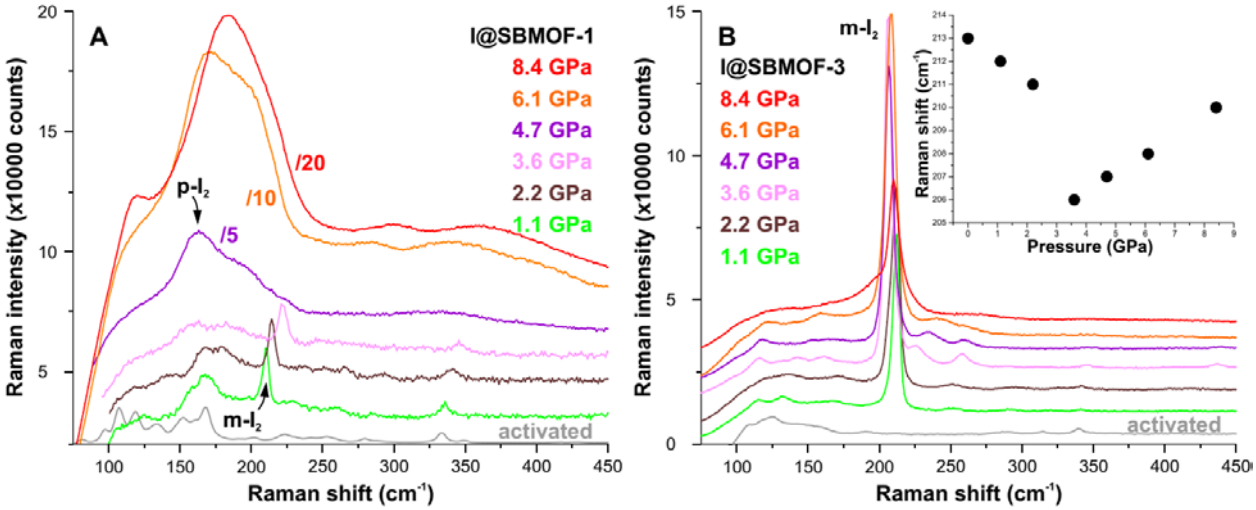


**Figure 3**. Raman spectra of I@SBMOF-1 (**A**) and I@SBMOF-3 (**B**) upon compression to 8.4 GPa collected using the 785-nm excitation. In (**A**): the intensity of the Raman spectra shown in purple (4.7 GPa), orange (6.1 GPa), and red (8.4 GPa) has been divide by five, ten, and twenty, respectively. The spectra at 2.2 and 3.6 GPa are offset vertically by 1000 and 2000 counts for clarity. In (**B**): All Raman spectra of I@SBMOF-3 are offset vertically for clarity. The inset shows the Raman shift of m-$I_2$ in I@SBMOF-3 versus pressure. In (**A**) and (**B**): Raman spectra of activated SBMOF-1 and SBMOF-3 at 1 atm are shown in grey.

Raman spectra of I@SBMOF-3 collected in the same high-pressure run are all dominated by the m-$I_2$ peak (Fig. 3B). The frequency of m-$I_2$ decreases up to 3.6 GPa with an average slope of -2.4 $cm^{-1}$/GPa. The negative frequency shift is quite unusual as it indicates loosening of the I-I bond strength with increasing pressure. However, a very similar negative shift has been reported in solid $I_2$ (-2.1 $cm^{-1}$/GPa) at pressures below ~3 GPa.[41] Interestingly, the negative frequency

shift of the I-I stretching vibration in I@SBMOF-3 is reversed at $P > 3.6$ GPa (Fig. 3B, inset). Again, a similar crossover in the sign of $dv/dP$ has been observed in solid $I_2$ at $P$ ~3 GPa.[41] The crossover indicates that the electronic structure of iodine in I@SBMOF-3 is governed by several competing factors such as a CT-induced weakening and pressure-induced strengthening of the bond; the latter apparently wins. The intensity of the m-$I_2$ band in the Raman spectra of I@SBMOF-3 increases steadily up to 6.1 GPa but is halved at 8.4 GPa due to the appearance of a low frequency shoulder at ~190-200 $cm^{-1}$.

To gain insights into the compression mechanisms of iodine-loaded SBMOF-1 and SBMOF-3 we recorded PXRD patterns upon compression to ~3 GPa followed by decompression to 1 atm (Fig. 4). I@SBMOF-1 is prone to amorphization as evidenced by its broadened XRD peaks already at 1.1 GPa. Interestingly, the peak at ~1.2° 2Θ, which is a combination of $10\bar{1}$ and 002 Bragg reflections, splits into these two components. Such splitting can only be attributed to framework flexing, which is enabled by the flexible C-S-C hinge in the center of the *sdb* linker and carbonyls on its ends, resulting in the increased $\beta$ angle from its 1 atm value of ~100 to ~110° at 1.1 GPa. Framework flexing is characteristic of MOFs with compliant 'wine-rack' topologies[45-50] of which SBMOF-1 is a representative (Fig. 1B). Unfortunately, the corresponding powder XRD patterns are considerably broadened and do not allow for structure refinement at high pressure. The apparent pressure-induced disorder in I@SBMOF-1 is fully reversible upon decompression to 1 atm as revealed by PXRD and confirmed by Raman spectroscopy, unlike many other MOFs with irreversible pressure-induced transformations.[50-51] The reversibility not only suggests that the long range order is restored upon decompression, but also that pressure-induced changes in the short range atomic distribution are gradual and the overall framework topology is preserved at high pressure.

I@SBMOF-3 remains crystalline up to at least 3.4 GPa (Fig. 4B). The angular positions of the 110 and 220 reflections cross over upon compression to 3.4 GPa, suggesting framework flexing along the *a* and *b* directions (Fig. 1D). Refining the I@SBMOF-3 unit cell at 3.4 GPa we obtain a 4.3 % reduction in *a* and 7.4 % increase in *b*. The apparent negative linear compressibility of I@SBMOF-3 is typical of compliant 'wine-rack' MOFs.[45-50]

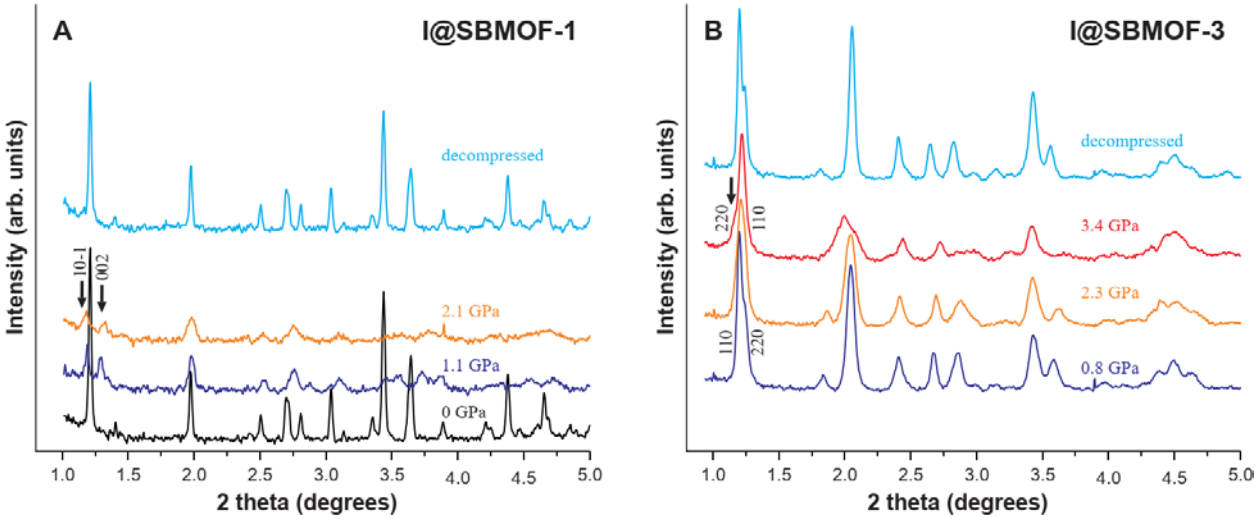


**Figure 4.** Powder x-ray diffraction patterns of I@SBMOF-1 (**A**) and I@SBMOF-3 (**B**) over a compression-decompression cycle. The x-ray wavelength is 0.2367 Å. The patterns were offset vertically for clarity.

## 4. DISCUSSION

Spectroscopic data suggest a crossover in the electronic structure of iodine in I@SBMOF-1 at ~3.5 GPa (Fig. 2A and 3A). In contrast, the character of iodine in I@SBMOF-3 remains largely unchanged up to at least 8.4 GPa (Fig. 2B and 3B). Table 1 summarizes the main observations of this study.

**Table 1.** Summary of major observations in I@SBMOFs upon compression

| Technique: | I@SBMOF-1 | I@SBMOF-3 |
|---|---|---|
| VIS spectroscopy | Fixed position of absorption edge @ $P < 3.4$ GPa<br>Red-shift of absorption edge @ $P \geq 3.4$ GPa<br>500-nm band diminishing @ $P \geq 3.4$ GPa<br>New bands (455 and 600 nm) @ $P \geq 4.8$ GPa | Fixed position of absorption edge in the studied $P$ range<br>500-nm band persists in the studied $P$ range |
| Raman spectroscopy | Strong positive $P$-shift of m-$I_2$ band<br>m-$I_2$ band not resolved @ $P > 3.6$ GPa<br>Irreversible p-$I_2$ band @ $P > 3.6$ GPa<br>Resonance Raman for p-$I_2$<br>New band at ~110 $cm^{-1}$ at 8.4 GPa | Negative $P$-shift of m-$I_2$ band @ $P \leq 3.6$ GPa<br>Positive $P$-shift of m-$I_2$ band @ $P \geq 3.6$ GPa<br>m-$I_2$ persists in the studied $P$ range |
| PXRD | Reversible framework flexing<br>Reversible amorphization @ P < 1 GPa | Reversible framework flexing<br>Crystalline up to at least 3.4 GPa |

The frequency of I-I stretching in I@SBMOF-1 is ~160-170 $cm^{-1}$ at $P = 3.6$ GPa (p-$I_2$ band), well below its gas value (~214 $cm^{-1}$).[40] Similar relatively low frequencies (150-180 $cm^{-1}$) of the I-I stretching vibration have been documented in the Raman spectra of polyiodides[42-43, 52] and iodine solutions in strong organic donors[20, 43, 53]. The reduced frequency is due to the

increased electron density at the $\sigma_u^*$ orbital of $I_2$ and is a fingerprint of strong donor-$I_2$ interaction, regardless of the donor kind.[24, 43] Two principal donor-acceptor scenarios can be proposed for I@SBMOF-1 at $P$ > 3.6 GPa: (i) pressure-induced aggregation of iodine into polyiodide chains and (ii) pressure-enhanced CT between $I_2$ and phenyl of the *sdb* linker.

The disappearance of the 500-nm band ($\pi_g^* \rightarrow \sigma_u^*$) in the absorption spectra of I@SBMOF-1 at $P$ > 3.4 GPa is consistent with these two principal types of donors as the occupancy of the $\sigma_u^*$ orbital is increased in both scenarios. Likewise, both CT scenarios provide a qualitative explanation for the pressure-intensified (or red-shifted) absorption edge. For example, the CT band in the absorption spectra of benzene-$I_2$ complex intensifies and red-shifts continuously from 288 nm (1 atm) to 293 nm (0.2 GPa)[54]. On the other hand, electronic spectra of $I_3^-$, the simplest polyiodide, have several broad absorption bands in the visible (centered at 565-590 and 440-460 nm) and UV range (< 350 nm)[55-56] as well as a distinct negative slope in the 350-800 nm range, just as the slope observed for I@SBMOF-1 at $P$ > 4.8 GPa (Fig. 2A). Therefore, the newly-formed absorption bands at 600 and 455 nm may signal for polyiodide formation but their unique assignment is challenging. The energy difference between the new bands (~ 5300 $cm^{-1}$) is characteristic of the spin-orbit splitting in $I_2$ (~5000 $cm^{-1}$)[37]; thus, the new bands may be due to a new type of iodine species in I@SBMOF-1 at high pressure. Suppose an $I_2^-$ anion ($^2\Sigma_{1/2u}$ ground state) as a result of severe CT at 7.5 GPa. The lowest energy excited state of $I_2^-$ would be split by spin-orbit coupling to the $^2\Pi_{3/2g}$ and $^2\Pi_{1/2g}$ states, both allowed by spectroscopic selection rules ($\Delta\Omega$=0, ±1). *Ab initio* calculations of the ground and excited electronic states of $I_2^-$ predicted a ~4700 $cm^{-1}$ gap between the $^2\Pi_{3/2g}$ – $^2\Pi_{1/2g}$ states.[57-58] This gap is consistent with the observed ~5300 $cm^{-1}$ difference, while the spectral positions of the new bands appear at lower wavelengths than that predicted by theory (1030 and 710 nm) for an equilibrium I-I separation of ~3.1 Å. The I-I bond length is likely shorter at high pressure, which may account for the discrepancy in the excitation energy. Although the spectroscopic properties of $I_2^-$ provide explanations for the new peaks at 600 and 455 nm, they do not help in discriminating between the proposed CT interactions.

The observed in PXRD pressure-induced increase in $\beta$ angle upon 'wine-rack' flexing is an efficient mechanism to overlap π electron density of the linker with diiodine molecular orbitals, enhancing phenyl···$I_2$ CT interactions. However, one should expect exactly the same in I@SBMOF-3 as a consequence of its similar 'wine-rack' topology. Apparently, that is not the case as I@SBMOF-3 does not show any increase in the strength of donor···$I_2$ interaction and, as a consequence, the molecular character of $I_2$ is preserved up to at least 8.4 GPa. Why would two MOFs that are based on the same linker and exhibit similar pressure-induced pore flexing show such severe differences in their interaction with iodine?

The efficiency of any CT interaction depends critically not only on the donor-acceptor distance but also on their molecular orbital overlap.[21] Iodine in the straight channels of I@SBMOF-1 has the ability to interact with neighboring iodine species through a direct $\sigma_u^* - \sigma_u^*$ overlap, which is achieved when $I_2$ molecular axes are aligned with the channel. Importantly, polyiodine building blocks ($I^-$, $I_3^-$, and $I_2$) are prone to catenation and in many cases form linear or quasi-linear polyiodides structures.[24, 59] In contrast, molecular orbital overlap in the sinusoidal channel of I@SBMOF-3 would be geometrically suppressed. The following spectroscopic and crystallographic arguments suggest that iodine in I@SBMOF-1 irreversibly forms 1D polyiodide chains.

The fixed spectral position of the absorption edge in I@SBMOF-1 at $P < 3.4$ GPa suggests that compression to 3.4 GPa does not enhance CT to iodine, which is also consistent with the nearly-fixed spectral position of the 500-nm band.[16, 54] At $P \geq 3.4$ GPa, however, the abrupt red-shift of the absorption edge clearly signals for an enhanced CT. Shortening of the phenyl$\cdots I_2$ distance with pressure, and therefore enhancement of their CT interaction, must be gradual upon 'wine-rack' flexing, inconsistent with the observed discontinuous position of the absorption edge. On the other hand, the nearly perpendicular orientation of $I_2$ to the phenyl ring in I@SBMOF-1 at 1 atm[10] precludes CT between neighboring $I_2$ molecules because of the lack of $\sigma_u^* - \sigma_u^*$ overlap. Rotation of $I_2$ molecules upon 'wine-rack' flexing would produce an abrupt increase in $I_2$-$I_2$ CT due to the $\sigma_u^* - \sigma_u^*$ molecular orbital overlap along the straight channel.

In the crystal structure of I@SBMOF-1, the centers of neighboring $I_2$ molecules are separated by 5.567 Å (at 1 atm) as templated by the unit cell repetition along the channel direction (Fig. 1A).[10] Upon pressure-induced 'wine-rack' flexing, rotation of discrete $I_2$ units minimizes the repulsive interaction of its $\pi_g^*$ (HOMO) with the π electron density of the linker. Iodine molecules aligned along the SBMOF-1 channel would be separated by ~2.9 Å, assuming initial I-I bond length (2.647 Å) is unaltered upon molecular rotation.[10] However, the $I_2\cdots I_2$ separation must be smaller than 2.9 Å because the CT interaction of neighboring $I_2$ molecules would inevitably loosen the intramolecular bond. Allowing for that, we obtain an extended 1D polyiodide chain in the I@SBMOF-1 channel with I-I bond of ~2.8 Å (Fig. 5). Such relatively long intramolecular I-I bond as well as the short $I_2\cdots I_2$ distance are characteristic of polyioides.[24, 56, 59-60] Raman spectroscopy provides an independent check on this qualitative scenario as the frequency of I-I stretching vibration correlates linearly with the I-I bond length[42-43], predicting exactly 2.8 Å based on the frequency of p-$I_2$ (160 $cm^{-1}$ in decompressed I@SBMOF-1).

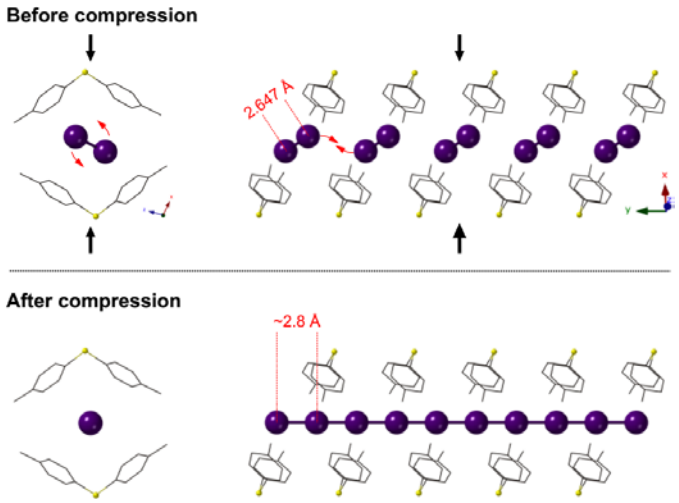


**Figure 5.** A spectroscopic model of the pressure-induced iodine polymerization in I@SBMOF-1. Black arrows depict the main flexing direction of the I@SBMOF-1 unit cell.

The framework of I@SBMOF-3 provides a larger dioiodine intermolecular distance of ~3.2 Å, outside the range of the $I_2 \cdots I_2$ distances in polyiodides deposited in the Cambridge Structural Database.[60] The sinusoidal channel of I@SBMOF-3 is also incommensurate with the formation of linear polyiodides. The very persistence of m-$I_2$ band in the Raman spectra of I@SBMOF-3 up to 8.4 GPa indicates that polyiodides are not formed in this MOF. As such, a sluggish CT to the $\sigma_u^*$ orbital of $I_2$, as signified by the negative frequency shift of the m-$I_2$ band at $P \leq 3.6$ GPa (Fig. 3B, inset), can only result from the iodine···phenyl interaction. This spectroscopic behavior can be viewed as a reference for a framework-to-iodine donor-acceptor exchange in 'wine-rack' MOFs. Raman spectra of I@SBMOF-1 do not follow this model trend: the m-$I_2$ band in I@SBMOF-1 shows a rapid pressure-induced stiffening at $P \leq 3.6$ GPa, indicating that any CT interactions in this pressure range are not important. The abrupt disappearance of the m-$I_2$ peak and a concurrent rise of the p-$I_2$ band at $P > 3.6$ GPa mark a crossover to iodine perturbed by CT. Given the similarities in pore size, chemistry, and pressure-flexing of I@SBMOF-1 and I@SBMOF-3, the sudden emergence of CT in I@SBMOF-1 is consistent with the formation of polyiodides at high pressure.

Finally, CT must affect not only the electron density and corresponding force constants of the acceptor but also the donor. For example, an upshift (~10 $cm^{-1}$) of the C=C stretching frequency in carbon nanotubes has been observed upon iodine intercalation.[61] However, the Raman shift of the C=C stretching in I@SBMOF-1 and I@SBMOF-3 has a similar response to high pressure and does not show discontinuities at $P$ ~3.5 GPa (Suppl. Fig. S3). Therefore, the magnitude of iodine···phenyl CT interaction is comparable across the studied MOFs and shows little variation with pressure, consistent with the polyiodides formation.

Previous studies provided crystallographic evidence for polyiodide speciation of iodine in MOFs that can lead to a very efficient iodine packing and its exceptional storage density.[9, 26] Here we reported independent spectroscopic evidence for polyiodide formation in MOFs at plausible conditions, such as the channel topology that allows templating iodine molecules into a 1D polyiodide chain though a direct overlap of their molecular orbitals. Our work suggests that channel topology must be considered in the rational design of MOFs for radioactive iodine removal. In addition, stabilization of extended polyiodides within MOFs offers new routes for the synthesis of exotic compounds with highly attractive technological properties, such 1D semiconductors and metals[62-63], nonlinear optical devises[26], and stimuli-responsive materials[64].

## 5. CONCLUSIONS

Herein we demonstrated that the electronic structure of iodine shows a contrasting response to high pressure in the channels of two MOFs that are similar in their pore size, its chemistry and pressure-flexing. In the straight channel of I@SBMOF-1, iodine molecules are perturbed by CT interaction to form 1D polyiodide chains along the channel. In contrast, iodine in I@SBMOF-3 appears to be shielded from CT interactions with neighboring iodine molecules by the sinusoidal shape of its channel. This work underscores the importance of channel topology of porous solids for the chemical state of the adsorbates with implications for an *ad hoc* design of MOFs.

## ASSOCIATED CONTENT

This material is available free of charge via the Internet at http://pubs.acs.org. Supporting Information. Absorption spectra of activated SBMOF-1 (Fig. S1), Raman spectra of I@SBMOF-1 over a full compression-decompression cycle (Fig. S2), Raman shift of the C=C symmetric stretching in I@SBMOF-1 and I@SBMOF-3 versus pressure (Fig. S3).

## AUTHOR INFORMATION

**Corresponding author:**

*E-mail: sergey.lobanov@gfz-potsdam.de

**Author contributions:**

The manuscript was written with contributions of all authors.

## ACKNOWLEDGMENTS

This research used beamline X-ray Powder Diffraction (XPD) beamline of the National Synchrotron Light Source II, a U.S. Department of Energy (DOE) Office of Science User

Facility operated for the DOE Office of Science by Brookhaven National Laboratory under Contract No. DE-SC0012704. A.F.G. acknowledges support of NSF EAR 1763287. Work at the beamline was also supported by the Joint Photon Sciences Institute, an entity funded by the office of the provost, Stony Brook University. We thank Yuri Janssen for his assistance with optical measurements.

## Reference

1. Furukawa, H.; Cordova, K. E.; O'Keeffe, M.; Yaghi, O. M. The Chemistry and Applications of Metal-Organic Frameworks. *Science* **2013,** *341*, 1230444.
2. DeCoste, J. B.; Peterson, G. W. Metal-Organic Frameworks for Air Purification of Toxic Chemicals. *Chem. Rev.* **2014,** *114*, 5695-5727.
3. Soelberg, N. R.; Garn, T. G.; Greenhalgh, M. R.; Law, J. D.; Jubin, R.; Strachan, D. M.; Thallapally, P. K. Radioactive Iodine and Krypton Control for Nuclear Fuel Reprocessing Facilities. *Sci. Technol. Nucl. Install.* **2013,** *2013*, 1-12.
4. Sava, D. F.; Rodriguez, M. A.; Chapman, K. W.; Chupas, P. J.; Greathouse, J. A.; Crozier, P. S.; Nenoff, T. M. Capture of Volatile Iodine, a Gaseous Fission Product, by Zeolitic Imidazolate Framework-8. *J. Am. Chem. Soc.* **2011,** *133*, 12398-12401.
5. Sava, D. F.; Chapman, K. W.; Rodriguez, M. A.; Greathouse, J. A.; Crozier, P. S.; Zhao, H. Y.; Chupas, P. J.; Nenoff, T. M. Competitive $I_2$ Sorption by Cu-BTC from Humid Gas Streams. *Chem. Mater.* **2013,** *25*, 2591-2596.
6. Falaise, C.; Volkringer, C.; Facqueur, J.; Bousquet, T.; Gasnot, L.; Loiseau, T. Capture of Iodine in Highly Stable Metal-Organic Frameworks: A Systematic Study. *Chem. Commun.* **2013,** *49*, 10320-10322.
7. Yao, R. X.; Cui, X.; Jia, X. X.; Zhang, F. Q.; Zhang, X. M. A Luminescent Zinc(II) Metal-Organic Framework (MOF) with Conjugated π-Electron Ligand for High Iodine Capture and Nitro-Explosive Detection. *Inorg. Chem.* **2016,** *55*, 9270-9275.
8. Li, B.; Dong, X.; Wang, H.; Ma, D.; Tan, K.; Jensen, S.; Deibert, B. J.; Butler, J.; Cure, J.; Shi, Z., et al. Capture of Organic Iodides from Nuclear Waste by Metal-Organic Framework-Based Molecular Traps. *Nat. Commun.* **2017,** *8*, 485.
9. Zhang, X. R.; da Silva, I.; Godfrey, H. G. W.; Callear, S. K.; Sapchenko, S. A.; Cheng, Y. Q.; Vitorica-Yrezabal, I.; Frogley, M. D.; Cinque, G.; Tang, C. C., et al. Confinement of Iodine Molecules into Triple-Helical Chains within Robust Metal-Organic Frameworks. *J. Am. Chem. Soc.* **2017,** *139*, 16289-16296.
10. Banerjee, D.; Chen, X.; Lobanov, S. S.; Plonka, A. M.; Chan, X.; Daly, J. A.; Kim, T.; Thallapally, P. K.; Parise, J. B. Iodine Adsorption in Metal Organic Frameworks in the Presence of Humidity. *ACS Appl. Mater. Interfaces* **2018,** *10*, 10622-10626.
11. Ma, S. L.; Islam, S. M.; Shim, Y.; Gu, Q. Y.; Wang, P. L.; Li, H.; Sun, G. B.; Yang, X. J.; Kanatzidis, M. G. Highly Efficient Iodine Capture by Layered Double Hydroxides Intercalated with Polysulfides. *Chem. Mater.* **2014,** *26*, 7114-7123.
12. Yan, Z.; Yuan, Y.; Tian, Y.; Zhang, D.; Zhu, G. Highly Efficient Enrichment of Volatile Iodine by Charged Porous Aromatic Frameworks with Three Sorption Sites. *Angew. Chem. Int. Ed.* **2015,** *54*, 12733-12737.
13. Jie, K. C.; Zhou, Y. J.; Li, E. R.; Li, Z. T.; Zhao, R.; Huang, F. H. Reversible Iodine Capture by Nonporous Pillar[6]arene Crystals. *J. Am. Chem. Soc.* **2017,** *139*, 15320-15323.
14. Hughes, J. T.; Sava, D. F.; Nenoff, T. M.; Navrotsky, A. Thermochemical Evidence for Strong Iodine Chemisorption by ZIF-8. *J. Am. Chem. Soc.* **2013,** *135*, 16256-16259.

15. Wang, Z.; Huang, Y.; Yang, J.; Li, Y. S.; Zhuang, Q. X.; Gu, J. L. The Water-Based Synthesis of Chemically Stable Zr-Based Mofs Using Pyridine-Containing Ligands and Their Exceptionally High Adsorption Capacity for Iodine. *Dalton Trans.* **2017,** *46*, 7412-7420.
16. Benesi, H. A.; Hildebrand, J. H. A Spectrophotometric Investigation of the Interaction of Iodine with Aromatic Hydrocarbons. *J. Am. Chem. Soc.* **1949,** *71*, 2703-2707.
17. Mulliken, R. S. Molecular Compounds and Their Spectra. III. The Interaction of Electron Donors and Acceptors. *J. Phys. Chem.* **1952,** *56*, 801-822.
18. Mulliken, R. S. Structures of Complexes Formed by Halogen Molecules with Aromatic and with Oxygenated Solvents. *J. Am. Chem. Soc.* **1950,** *72*, 600-608.
19. Hastings, S. H.; Franklin, J. L.; Schiller, J. C.; Matsen, F. A. Molecular Complexes Involving Iodine. *J. Am. Chem. Soc.* **1953,** *75*, 2900-2905.
20. Klaboe, P. Raman Spectra of Some Iodine Bromine and Iodine Monochloride Charge-Transfer Complexes in Solution. *J. Am. Chem. Soc.* **1967,** *89*, 3667-3676.
21. Mulliken, R. S. Molecular Compounds and Their Spectra. II. *J. Am. Chem. Soc.* **1952,** *74*, 811-824.
22. Sawamura, S.; Taniguchi, Y.; Suzuki, K. Effect of Pressure on Iodine Complexes. II. Absorption-Spectra of the Charge-Transfer Bands with Diethyl Ether, Diethyl Sulfide, and Diethyl Selenide in Heptane. *Bull. Chem. Soc. Jpn.* **1979,** *52*, 284-286.
23. Kenichi, T.; Kyoko, S.; Hiroshi, F.; Mitsuko, O. Modulated Structure of Solid Iodine During Its Molecular Dissociation under High Pressure. *Nature* **2003,** *423*, 971-974.
24. Svensson, P. H.; Kloo, L. Synthesis, Structure, and Bonding in Polyiodide and Metal Iodide-Iodine Systems. *Chem. Rev.* **2003,** *103*, 1649-1684.
25. Grochala, W.; Hoffmann, R.; Feng, J.; Ashcroft, N. W. The Chemical Imagination at Work in Very Tight Places. *Angew. Chem. Int. Ed.* **2007,** *46*, 3620-3642.
26. Yin, Z.; Wang, Q. X.; Zeng, M. H. Iodine Release and Recovery, Influence of Polyiodide Anions on Electrical Conductivity and Nonlinear Optical Activity in an Interdigitated and Interpenetrated Bipillared-Bilayer Metal-Organic Framework. *J. Am. Chem. Soc.* **2012,** *134*, 4857-4863.
27. Hu, X. L.; Sun, C. Y.; Qin, C.; Wang, X. L.; Wang, H. N.; Zhou, E. L.; Li, W. E.; Su, Z. M. Iodine-Templated Assembly of Unprecedented 3d-4f Metal-Organic Frameworks as Photocatalysts for Hydrogen Generation. *Chem. Commun.* **2013,** *49*, 3564-3566.
28. Plonka, A. M.; Banerjee, D.; Woerner, W. R.; Zhang, Z. J.; Li, J.; Parise, J. B. Effect of Ligand Geometry on Selective Gas-Adsorption: The Case of a Microporous Cadmium Metal Organic Framework with a V-Shaped Linker. *Chem. Commun.* **2013,** *49*, 7055-7057.
29. Banerjee, D.; Zhang, Z.; Plonka, A. M.; Li, J.; Parise, J. B. A Calcium Coordination Framework Having Permanent Porosity and High $CO_2/N_2$ Selectivity. *Cryst. Growth Des.* **2012,** *12*, 2162-2165.
30. Dewaele, A.; Torrent, M.; Loubeyre, P.; Mezouar, M. Compression Curves of Transition Metals in the Mbar Range: Experiments and Projector Augmented-Wave Calculations. *Phys. Rev. B.* **2008,** *78*, 104102.
31. Goncharov, A. F.; Beck, P.; Struzhkin, V. V.; Haugen, B. D.; Jacobsen, S. D. Thermal Conductivity of Lower-Mantle Minerals. *Phys. Earth Planet. Inter.* **2009,** *174*, 24-32.
32. Goncharov, A. F.; Lobanov, S. S.; Tan, X.; Hohensee, G. T.; Cahill, D. G.; Lin, J. F.; Thomas, S. M.; Okuchi, T.; Tomioka, N. Experimental Study of Thermal Conductivity at High Pressures: Implications for the Deep Earth's Interior. *Phys. Earth Planet. Inter.* **2015,** *247*, 11-16.
33. Hammersley, A. P.; Svensson, S. O.; Hanfland, M.; Fitch, A. N.; Hausermann, D. Two-Dimensional Detector Software: From Real Detector to Idealised Image or Two-Theta Scan. *High Pressure Research* **1996,** *14*, 235-248.
34. Mulliken, R. S. Iodine Revisited. *J. Chem. Phys.* **1971,** *55*, 288-309.

35. Tellinghuisen, J. Resolution of Visible-Infrared Absorption Spectrum of $I_2$ into Three Contributing Transitions. *J. Chem. Phys.* **1973,** *58*, 2821-2834.
36. Gray, R. I.; Luckett, K. M.; Tellinghuisen, J. Component Analysis of the Visible Absorption Spectra of $I_2$ and $Br_2$ in Inert Solvents: A Critique of Band Decomposition by Least-Squares Fitting. *J. Phys. Chem. A* **2001,** *105*, 11183-11191.
37. Tellinghuisen, J. Analysis of the Visible Absorption Spectrum of $I_2$ in Inert Solvents Using a Physical Model. *J. Phys. Chem. A* **2012,** *116*, 391-398.
38. Grozema, F. C.; Zijlstra, R. W. J.; Swart, M.; van Duijnen, P. T. Iodine-Benzene Charge-Transfer Complex: Potential Energy Surface and Transition Probabilities Studied at Several Levels of Theory. *Int. J. Quantum. Chem.* **1999,** *75*, 709-723.
39. McConnell, H.; Ham, J. S.; Platt, J. R. Regularities in the Spectra of Molecular Complexes. *J. Chem. Phys.* **1953,** *21*, 66-70.
40. Kiefer, W.; Bernstein, H. J. Resonance Raman Spectroscopic Study on Iodine in Various Organic Solvents: Spectroscopic Constants and Halfband Widths of the $I_2$ Vibration. *J. Raman Spectrosc.* **1973,** *1*, 417-431.
41. Olijnyk, H.; Li, W.; Wokaun, A. High-Pressure Studies of Solid Iodine by Raman-Spectroscopy. *Phys. Rev. B* **1994,** *50*, 712-716.
42. Deplano, P.; Devillanova, F. A.; Ferraro, J. R.; Mercuri, M. L.; Lippolis, V.; Trogu, E. F. FT-Raman Study on Charge-Transfer Polyiodide Complexes and Comparison with Resonance Raman Results. *Appl. Spectrosc.* **1994,** *48*, 1236-1241.
43. Deplano, P.; Devillanova, F. A.; Ferraro, J. R.; Isaia, F.; Lippolis, V.; Mercuri, M. L. On the Use of Raman Spectroscopy in the Characterization of Iodine in Charge-Transfer Complexes. *Appl. Spectrosc.* **1992,** *46*, 1625-1629.
44. Howard, W. F.; Andrews, L. Raman Spectra of Alkali Metal-Iodine Matrix Reaction Products. Resonance Raman Spectrum of Iodine Molecular Anion, $I_2^-$. *J. Am. Chem. Soc.* **1975,** *97*, 2956-2959.
45. Li, W.; Probert, M. R.; Kosa, M.; Bennett, T. D.; Thirumurugan, A.; Burwood, R. P.; Parinello, M.; Howard, J. A. K.; Cheetham, A. K. Negative Linear Compressibility of a Metal-Organic Framework. *J. Am. Chem. Soc.* **2012,** *134*, 11940-11943.
46. Ogborn, J. M.; Collings, I. E.; Moggach, S. A.; Thompson, A. L.; Goodwin, A. L. Supramolecular Mechanics in a Metal-Organic Framework. *Chem. Sci.* **2012,** *3*, 3011-3017.
47. Ortiz, A. U.; Boutin, A.; Fuchs, A. H.; Coudert, F. X. Metal-Organic Frameworks with Wine-Rack Motif: What Determines Their Flexibility and Elastic Properties? *J. Chem. Phys.* **2013,** *138*, 174703.
48. Sarkisov, L.; Martin, R. L.; Haranczyk, M.; Smit, B. On the Flexibility of Metal-Organic Frameworks. *J. Am. Chem. Soc.* **2014,** *136*, 2228-2231.
49. Cai, W. Z.; Katrusiak, A. Giant Negative Linear Compression Positively Coupled to Massive Thermal Expansion in a Metal-Organic Framework. *Nat. Commun.* **2014,** *5*, 4337.
50. McKellar, S. C.; Moggach, S. A. Structural Studies of Metal-Organic Frameworks under High Pressure. *Acta Cryst. B* **2015,** *71*, 587-607.
51. Spencer, E. C.; Kiran, M. S. R. N.; Li, W.; Ramamurty, U.; Ross, N. L.; Cheetham, A. K. Pressure-Induced Bond Rearrangement and Reversible Phase Transformation in a Metal-Organic Framework. *Angew. Chem. Int. Ed.* **2014,** *53*, 5583-5586.
52. Ferraro, J. R.; Martin, K.; Furlani, A.; Russo, M. V. Vibrational Spectroscopy of Iodine-Doped Poly(Phenyl)Acetylene. *Appl. Spectrosc.* **1984,** *38*, 267-270.
53. Tassaing, T.; Besnard, M. Ionization Reaction in Iodine/Pyridine Solutions: What Can We Learn from Conductivity Measurements, Far-Infrared Spectroscopy, and Raman Scattering? *J. Phys. Chem. A* **1997,** *101*, 2803-2808.

54. Ham, J. The Spectra of Iodine Solutions. II. The Effects of High Pressures Upon Iodine Complexes. *J. Am. Chem. Soc.* **1954,** *76*, 3881-3885.
55. Gabes, W.; Stufkens, D. J. Electronic Absorption Spectra of Symmetrical and Asymmetrical Trihalide Ions. *Spectrochim. Acta A* **1974,** *A 30*, 1835-1841.
56. Mizuno, M.; Tanaka, J.; Harada, I. Electronic Spectra and Structures of Polyiodide Chain Complexes. *J. Phys. Chem.* **1981,** *85*, 1789-1794.
57. Maslen, P. E.; Faeder, J.; Parson, R. Ab Initio Calculations of the Ground and Excited States of $I_2^-$ and $ICl^-$. *Chem. Phys. Lett.* **1996,** *263*, 63-72.
58. Faeder, J.; Delaney, N.; Maslen, P. E.; Parson, R. Modeling Structure and Dynamics of Solvated Molecular Ions: Photodissociation and Recombination in $I_2^-(CO_2)_n$. *Chem. Phys.* **1998,** *239*, 525-547.
59. Blake, A. J.; Devillanova, F. A.; Gould, R. O.; Li, W. S.; Lippolis, V.; Parsons, S.; Radek, C.; Schroder, M. Template Self-Assembly of Polyiodide Networks. *Chem. Soc. Rev.* **1998,** *27*, 195-205.
60. Kloo, L.; Rosdahl, J.; Svensson, P. H. On the Intra- and Intermolecular Bonding in Polyiodides. *Eur. J. Inorg. Chem.* **2002**, 1203-1209.
61. Grigorian, L.; Williams, K. A.; Fang, S.; Sumanasekera, G. U.; Loper, A. L.; Dickey, E. C.; Pennycook, S. J.; Eklund, P. C. Reversible Intercalation of Charged Iodine Chains into Carbon Nanotube Ropes. *Phys. Rev. Lett.* **1998,** *80*, 5560-5563.
62. Perlstein, J. H. ''Organic Metals'' - the Intermolecular Migration of Aromaticity. *Angew. Chem. Int. Ed.* **1977,** *16*, 519-534.
63. Komsa, H. P.; Senga, R.; Suenaga, K.; Krasheninnikov, A. V. Structural Distortions and Charge Density Waves in Iodine Chains Encapsulated inside Carbon Nanotubes. *Nano Lett.* **2017,** *17*, 3694-3700.
64. Ozaki, N.; Sakamoto, H.; Nishihara, T.; Fujimori, T.; Hijikata, Y.; Kimura, R.; Irle, S.; Itami, K. Electrically Activated Conductivity and White Light Emission of a Hydrocarbon Nanoring-Iodine Assembly. *Angew. Chem. Int. Ed.* **2017,** *56*, 11196-11202.

# TOC Graphic